



Article

The Synthesis Process and Thermal Stability of V₂C MXene

Meng Wu ^{1,2}, Bingxin Wang ^{1,2}, Qianku Hu ^{1,2}, Libo Wang ^{1,2}  and Aiguo Zhou ^{1,2,*} 

¹ School of Materials Science and Engineering, Henan Polytechnic University, Jiaozuo 454000, Henan, China; wumeng32323@163.com (M.W.); wbx0816@126.com (B.W.); hqk@hpu.edu.cn (Q.H.); wanglibo537@hpu.edu.cn (L.W.)

² Henan International Joint Research Laboratory for High-Performance Light Metallic Materials and Numerical Simulations, Henan Polytechnic University, Jiaozuo 454000, Henan, China

* Correspondence: zhouag@hpu.edu.cn

Received: 16 September 2018; Accepted: 18 October 2018; Published: 27 October 2018



Abstract: The effect of etching solution on the synthesis process of two-dimensional vanadium carbide (V₂C MXene) was researched. Three etching solutions were used to etch ternary carbide V₂AlC at 90 °C. The three solutions were: lithium fluoride + hydrochloric acid (LiF + HCl), sodium fluoride + hydrochloric acid (NaF + HCl), and potassium fluoride + hydrochloric acid (KF + HCl). It was found that only NaF + HCl solution was effective for synthesizing highly pure V₂C MXene. The existence of sodium (Na⁺) and chloridion (Cl⁻) in etching solution was essential for the synthesis. The thermal stability of the as-prepared V₂C MXene in argon or air was studied. From thermogravimetry and differential thermal analysis, V₂C MXene was found to be stable in argon atmosphere at a temperature of up to 375 °C. As the temperature increased, V₂C MXene was gradually oxidized to form nanoparticles composed of vanadium trioxide (V₂O₃) and a part of V₂C MXene was broken and transformed to vanadium carbide (V₈C₇) at 1000 °C. In air atmosphere, V₂C MXene was stable at 150 °C. At 1000 °C, V₂C MXene was oxidized to form vanadium pentoxide (V₂O₅).

Keywords: MXene; V₂C; synthesis; thermal stability

1. Introduction

In 2011, a novel two-dimensional (2D) transition metal carbide, Ti₃C₂, was synthesized by removing the Al layer from titanium aluminum carbide (Ti₃AlC₂) in hydrofluoric acid (HF) [1]. The precursor, Ti₃AlC₂, is a member of MAX phases, which is a family of ternary carbide or nitride with the formula M_{n+1}AX_n, where M is a transition metal, A is the main-group element, and X is either or both C and N. Inspired by the synthesis of Ti₃C₂, similar 2D materials, such as Ti₂C [2], Mo₂C [3], Nb₂C, and V₂C [4], were synthesized. These 2D materials are made by removing the A element from MAX phases and have a similar structure to graphene, and are thus named MXenes. Because MXenes are made in aqueous solution of F⁻, due to the high surface energy, the surface of MXenes are always terminated with F/OH/O groups [5–7]. T_x was used to denote the surface terminated functional groups. Thus, the chemical formula of Ti₃C₂ can be changed to Ti₃C₂T_x, and that of V₂C can be changed to V₂CT_x.

MXenes have many important applications in many fields, such as in the anode of a lithium-ion battery (LIB) [4,8–11] and the catalyst for the hydrogen evolution reaction (HER) [3,12,13]. Recently, based on theoretical calculation [14], V₂C MXene was found to have a better performance as an anode of LIB than many other MXenes. Additionally, many applications of V₂C MXene have been reported. V₂C MXene can be used as the positive electrode of sodium ion capacitors, showing good results for sodium ion capacitors [15]. V₂C MXene was reported to be used to capture CO₂ in the interlayer

space [16]. Furthermore, it was also found that V_2C MXene decorated with metals displays extremely high catalytic activity for the hydrogen evolution reaction (HER), which provides a new possibility for cost-effective alternatives to the noble metal Pt [6].

Although V_2C MXene theoretically has a much better performance than other MXenes, highly pure V_2C MXene is difficult to be made. This is because the formation energy of V_2C MXene is lower than that of other MXenes [17]. The common method employed to make MXenes has been to etch MAX phases precursor in HF solution at room temperature [1,5,18]. However, V_2C MXene made by this method has been shown to contain plenty of vanadium aluminum carbide (V_2AlC) precursor [4,15,19,20].

In 2017, we found a new method, sodium fluoride/hydrochloric acid ($NaF + HCl$) etching at 90 °C, to synthesize V_2C MXene. By that method, highly pure V_2C MXene with good Li storage properties was synthesized [21]. This work was inspired by a report on synthesizing Ti_3C_2 MXene by lithium fluoride/hydrochloric acid ($LiF + HCl$) etching [22]. Thus, a question was proposed. Why is $NaF+HCl$ rather than $LiF+HCl$ a suitable etchant? If NaF is replaced by LiF or other fluorides, can V_2C be synthesized? One of the purposes of this paper is to answer this question. Three fluorides were used to make etching solutions with HCl for V_2C MXene synthesis. The effects of these solutions on the etching process were clarified.

Because of the low formation energy, V_2C MXene is difficult to synthesize. For the same reason, V_2C MXene is highly unstable. Li et al., studied the thermal stability of Ti_3C_2 in oxygen and argon [23]. Zhou et al., studied the structural stability of Zr_3C_2 and Ti_3C_2 at elevated temperatures. Compared to Ti-based MXene, Zr_3C_2 exhibits relatively better high-temperature stability [24]. As the authors know, there is no report on the thermal stability of V_2C MXene. Therefore, another purpose of this paper is to study the thermal stability of V_2C MXene by thermal analysis.

2. Experimental

2.1. Syntheses of V_2C MXene

V_2C MXene was produced by immersing V_2AlC powders in etching solution. The V_2AlC powders were synthesized by the molten salt method [25] from vanadium powders (V, 99.6 wt.%, 325 mesh, Xingrongyuan Company, Beijing, China), aluminum powders (Al, 99.6 wt.%, 200 mesh, Xingrongyuan Company, Beijing, China), and graphite powders (C, 99.0 wt.%, 200 mesh, Jingchunshenghua Company, Shanghai, China). V, Al, and C powders were weighed according to the molar ratio of 2:1.2:1. Then, sodium chloride ($NaCl$) powders (99.5 wt.%, Yongda Company, Tianjin, China) were weighed according to the mass ratio of $(2V/1.2Al/C): NaCl = 1:1$. All powders were mixed by a ball mill machine for 12 h. Then, the mixtures of $2V/1.2Al/C$ and $NaCl$ were placed in an alumina crucible and put in a tube furnace. The samples were annealed in flowing Ar atmosphere (99%) at 1400 °C for 2 h. The obtained sample was crushed and sieved through a 500-mesh sieve to yield powders.

The etching solution was made by mixing fluoride with hydrochloric acid (HCl , 6 mol/L, Shuangshuang Chemical Company, Yantai, China). The fluoride was NaF (≥ 98 wt.%, Sinopharm Chemical Reagent Company, Beijing, China), LiF (≥ 98.5 wt.%, Guangfu Fine Chemical Research Institute, Tianjin, China), or KF (≥ 99 wt.%, Chemical Reagent Factory, Luoyang, China). The fluoride (2.00 g NaF , 1.24 g LiF or 4.48 g $KF \cdot 2H_2O$) was ultrasonic mixed with 40 mL HCl and 40 mL distilled water for 15 min, respectively. The mass difference of fluoride was used to obtain etching solution with the same molar concentration (0.6 mol/L). After that, 1.44 g V_2AlC powders were immersed in the solutions, and the solutions were then kept for 72 h at 90 °C with magnetic stirring. Thereafter, V_2C MXene powders were centrifugally separated from the etching solutions, and washed with deionized water and ethanol repeatedly to remove possible absorbed ions and remaining precursors. Before characterization, the obtained powders were dried in vacuum at 80 °C for 24 h.

The abbreviations and the corresponding full names of chemical substances that appear in this paper are listed in Table 1.

Table 1. Abbreviations and the corresponding full names of chemical substances.

Abbreviation	Full Name
V ₂ C MXene	two-dimensional vanadium carbide
V ₂ AlC	vanadium aluminum carbide
V ₂ O ₃	vanadium trioxide
V ₂ O ₅	vanadium pentoxide
V ₈ C ₇	vanadium carbide
NaV ₆ O ₁₅	sodium vanadium oxide
LiF	lithium fluoride
NaF	sodium fluoride
KF	potassium fluoride
HCl	hydrochloric acid
HF	hydrofluoric acid
NaCl	sodium chloride

2.2. Characterization

X-ray diffraction patterns of sample powders were obtained with an X-ray diffractometer (XRD; Rigaku, Smart-lab, Tokyo, Japan) with Cu K α radiation, $\lambda = 1.5406 \text{ \AA}$. A field emission scanning electron microscope (SEM; Merlin Compact, Carl Zeiss NTS GmbH, Jena, Germany) equipped with an energy dispersive spectroscope (EDS; X-Max^N, Oxford, UK) and a transmission electron microscope (TEM; JEOLJEM-2010, Tokyo, Japan) with an accelerating voltage of 200 kV were used to observe the microstructure morphology and element distribution of samples. Raman spectrum was recorded with a confocal spectrometer (Horiba JobinYvon, LabRAM HR800, Paris, France), using the 514.5 nm excitation of the argon laser at room temperature. The Raman spectral resolution was $<0.35 \text{ cm}^{-1}$.

The thermal stability of the sample was analyzed by a thermal analyzer (STA449C, Netzsch, Selb, Germany) with α -Al₂O₃ pans under argon/air flow with a heating rate of 5 °C/min from room temperature (RT) to 1000 °C. The thermogravimetric (TG) curve and differential thermal analysis (DTA) curve were obtained by this analysis.

3. Results and Discussion

3.1. Synthesis Process Analysis

The XRD patterns of V₂AlC samples before and after the etching in different solutions are shown in Figure 1.

In Figure 1, after V₂AlC powders are etched by LiF + HCl for 72 h, the peaks of V₂AlC still exist and very strong diffraction peaks of LiF appear. A weak peak appears at $2\theta \approx 9^\circ$, which belongs to newly formed V₂C MXene. However, the main diffraction peaks still belong to V₂AlC and LiF. Thus, LiF + HCl etching cannot make highly pure V₂C MXene. After etching in NaF + HCl solution, the diffraction peaks of V₂AlC completely disappear and a strong peak at 8.03° appears, corresponding to the (002) plane of V₂C MXene. This result indicates that Al was selectively etched off from V₂AlC and most V₂AlC had already been transformed to V₂C MXene. The *c* lattice parameter (*c*-LP) of V₂C calculated from the 2θ is 22.0 Å. The *c*-LP of V₂C MXene made by HF etching at RT was 19.8 Å [15]. Compared with that V₂C MXene, the V₂C made by this method has obviously larger *c*-LP and a higher purity. Thus, highly pure V₂C MXene can be made by NaF + HCl etching. However, after etching in KF + HCl solution, there were only the diffraction peaks of V₂AlC in the product; in other words, V₂AlC cannot be exfoliated in KF + HCl solution at 90 °C for 72 h.

From the above results, V₂AlC can only be effectively exfoliated in NaF + HCl solution. In the three etching solutions, the type and concentration of anions (F⁻ and Cl⁻) are the same and the concentration of cations is also the same. The only difference is the type of cation. Therefore, the type of cation is an important factor that affects the synthesis of V₂C MXene. For the radius of the three cations, $K^+ > Na^+ > Li^+$. However, in aqueous etching solution, the cations are hydrated. For the radius

of hydrated cations, $[\text{Li}(\text{H}_2\text{O})_x]^+ > [\text{Na}(\text{H}_2\text{O})_y]^+ > [\text{K}(\text{H}_2\text{O})_z]^+$ [26]. Thus, $[\text{Li}(\text{H}_2\text{O})_x]^+$, among the three hydrated cations, should have the largest ability to exfoliate V_2C MXene. However, LiF is hardly soluble in water, so the concentration of $[\text{Li}(\text{H}_2\text{O})_x]^+$ is the smallest, which can be confirmed by the LiF peaks in the XRD of Figure 1. Thus, $\text{LiF} + \text{HCl}$ can be used to exfoliate V_2AlC ; however, the exfoliation is not thorough. For $[\text{Na}(\text{H}_2\text{O})_y]^+$, the radius is larger than that of $[\text{K}(\text{H}_2\text{O})_z]^+$ and the concentration is much larger than that of $[\text{Li}(\text{H}_2\text{O})_x]^+$. Therefore, $[\text{Na}(\text{H}_2\text{O})_y]^+$ can be used to thoroughly exfoliate V_2AlC , and $\text{NaF} + \text{HCl}$ is the best etching solution for making V_2C MXene.

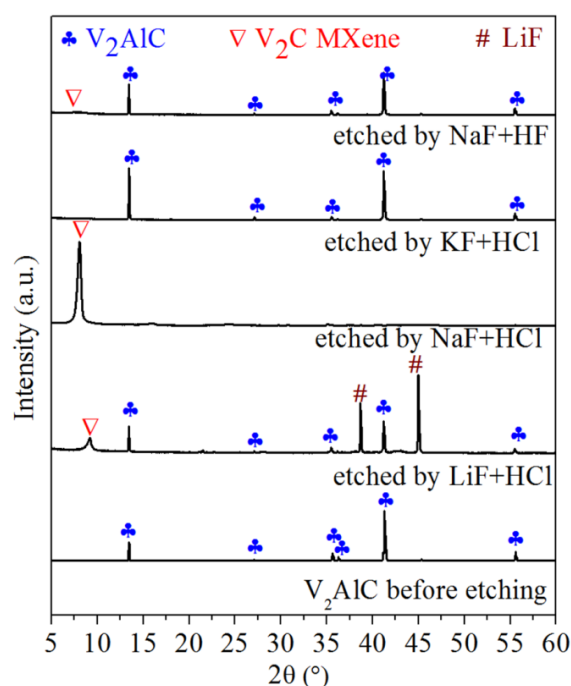


Figure 1. XRD patterns of V_2AlC samples before and after the etching in different solutions.

Initially, MXenes (Ti_3C_2 , Ti_2C , etc.) were synthesized in HF solution [1,27]. Thus, H^+ and F^- are considered to be essential for the synthesis of MXene. In order to reduce the toxicity and causticity of HF, fluoride salt ($\text{LiF}/\text{NaF}/\text{KF}$, etc.) + HCl was used to replace HF [21,28]. However, in this research, it is found that, for the V_2C synthesis, $\text{NaF} + \text{HCl}$ not only reduces the toxicity of HF, but also increases the exfoliating ability by providing Na^+ . Besides Na^+ , compared with HF, $\text{NaF} + \text{HCl}$ also provides Cl^- . Does the existence of Cl^- affect the synthesis? In order to investigate the influence of Cl^- , we conducted the following experiment: 1.44 g V_2AlC powders were soaked in $\text{NaF} + \text{HF}$ solution without Cl^- . This $\text{NaF} + \text{HF}$ solution was composed of 1 mL HF (48 mol/L, Aladdin Co., Shanghai, China), 99 mL distilled water, and 0.50 g NaF . The F^- concentration was 0.6 mol/L, consistent with the $\text{NaF} + \text{HCl}$ solution (0.6 mol/L). As shown in the top pattern of Figure 1, the main composition of the etched product in $\text{NaF} + \text{HF}$ was still V_2AlC . Thus, as is the same as the effect of Na^+ , H^+ , and F^- , the existence of Cl^- in etching solution is essential for the synthesis of highly pure V_2C MXene.

At this point, we do not clearly know the chemical reason why Cl^- is required in the etching. A possible reason is that the concentration of Na^+ is important for the exfoliation of V_2AlC . NaF has a better solubility in $\text{NaF} + \text{HCl}$ solution than that in $\text{NaF} + \text{HF}$ solution due to the concentration of F^- . Thus, $\text{NaF} + \text{HCl}$ has a better exfoliation ability than $\text{NaF} + \text{HF}$.

Table 2 lists the 2θ ($^\circ$) of the (002) peak of newly formed V_2C MXene by different methods and the intensity ratio of V_2C 's (002) peak to V_2AlC 's (002) peak ($I_{\text{MXene}}/I_{\text{MAX}}$). The $I_{\text{MXene}}/I_{\text{MAX}}$ for V_2C MXene etched by $\text{NaF} + \text{HCl}$ is 18.11, and this value is much higher than the value (1.00 or 0.22) of previously reported samples etched by HF at room temperature [4,19]. This means that the V_2C MXenes made by this method were much purer than the samples reported in previous literature.

Table 2. 2θ ($^\circ$) of the (002) peak of newly formed V_2C by different methods and the intensity ratio of V_2C 's (002) peak to V_2AlC 's (002) peak (I_{MXene}/I_{MAX}).

Etching Solution	2θ ($^\circ$) of (002) Peak	I_{MXene}/I_{MAX}
LiF + HCl	9.13	0.66
NaF + HCl	8.03	18.11
KF + HCl	-	-
NaF + HF	7.8	0.18
40% HF [19]	7.33	1.00
50% HF [4]	8.96	0.22

Figure 2a,b show the SEM images of V_2AlC and etched samples. As shown in Figure 2a, V_2AlC exhibits typical dense ceramic particles. As shown in Figure 2b, etched samples by NaF + HCl have a multi-layer stacked structure, and the inset has a typical 2D stack structure of MXene. Thus, exfoliation was achieved and quasi-2D MXene sheets were obtained by NaF + HCl etching. All the SEM results in Figure 2a,b agree well with the conclusions drawn from the XRD results in Figure 1.

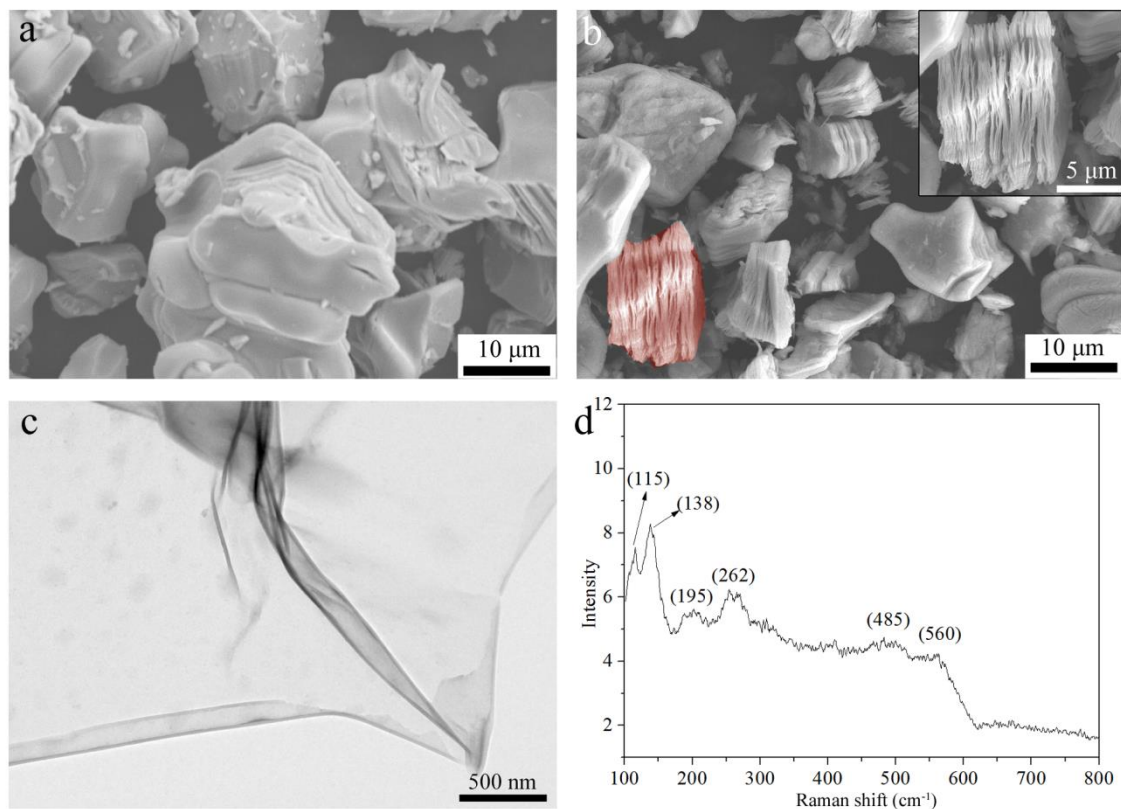


Figure 2. SEM (a,b) and TEM (c) images and Raman spectrum (d) of samples. (a) V_2AlC , (b–d) exfoliated product in NaF + HCl. The inset is an enlarged image of (b).

In order to determine the element content on the sample surface, the sample was analyzed by EDS. The EDS results of V_2AlC after being treated at $90^\circ C$ for 72 h in NaF and HCl solution indicated the presence of V, C, O, F, and small amounts of Al at an atomic ratio of 2.00:1.00:0.98:0.3:0.03, respectively. Assuming, conservatively, that the entirety of the Al signal originates from unreacted V_2AlC , the amount of Al would be around 0.59 wt.% after treatment. This indicates that only a very small part of V_2AlC had not been etched. This is more proof that highly pure V_2C MXene was successfully prepared.

Figure 2c is the TEM image of a piece of fully exfoliated V_2C sheet. From this image, the electron-transparent thin morphology and 2D structure of V_2C MXene are shown. Moreover,

the thin nanosheet is presented as flexible. Figure 2d is the Raman spectrum of V_2C MXene. The bands of V_2AlC at 158, 240, 257, and 361 cm^{-1} and weaker peaks near 413, 509, and 693 cm^{-1} [29,30] vanished and new bands appeared at 115, 138, 195, 262, 485, and 560 cm^{-1} . According to the theoretical work of Champagne et al. [30], the peak at 195 cm^{-1} corresponds to the E_g model of V_2CF_2 ; the peak at 262 cm^{-1} corresponds to the E_g model of V_2C ; the peak at 485 cm^{-1} corresponds to the E_g model of $V_2C(OH)_2$; and the peak at 560 corresponds to the A_{1g} model of V_2CF_2 and $V_2C(OH)_2$. The E_g model is due to the in-plane vibration of V atoms and the A_{1g} model is due to the out-of-plane vibration of V atoms. The two peaks at 115 and 138 cm^{-1} cannot currently be explained. Champagne et al. [30] reported similar results where, in the spectrum of V_2C MXene, sharp peaks of V_2AlC vanished. However, only two unsharp peaks at ~ 260 and ~ 410 cm^{-1} appeared in the spectrum. Thus, the spectrum in Figure 2d has more peaks that fit the theoretical prediction in [30]. The difference should be because the V_2C MXene samples were made by different methods (NaF + HCl high temperature etching in this paper and HF room temperature etching in [30]) and the samples had different terminations and impurities.

3.2. Thermal Stability Analysis

The TG curves and DTA curves of as-prepared V_2C MXene etched by NaF + HCl are shown in Figure 3a,b. In order to know the phase and morphology change at a high temperature, V_2C MXene samples were heat treated at different temperatures in Ar or air atmosphere. The XRD patterns of the sample before and after heat treatment are shown in Figure 3c,d. SEM micrographs are shown in Figure 4. Based on these results, the phase change of V_2C MXene from room temperature (RT) to 1000 $^{\circ}C$ is discussed.

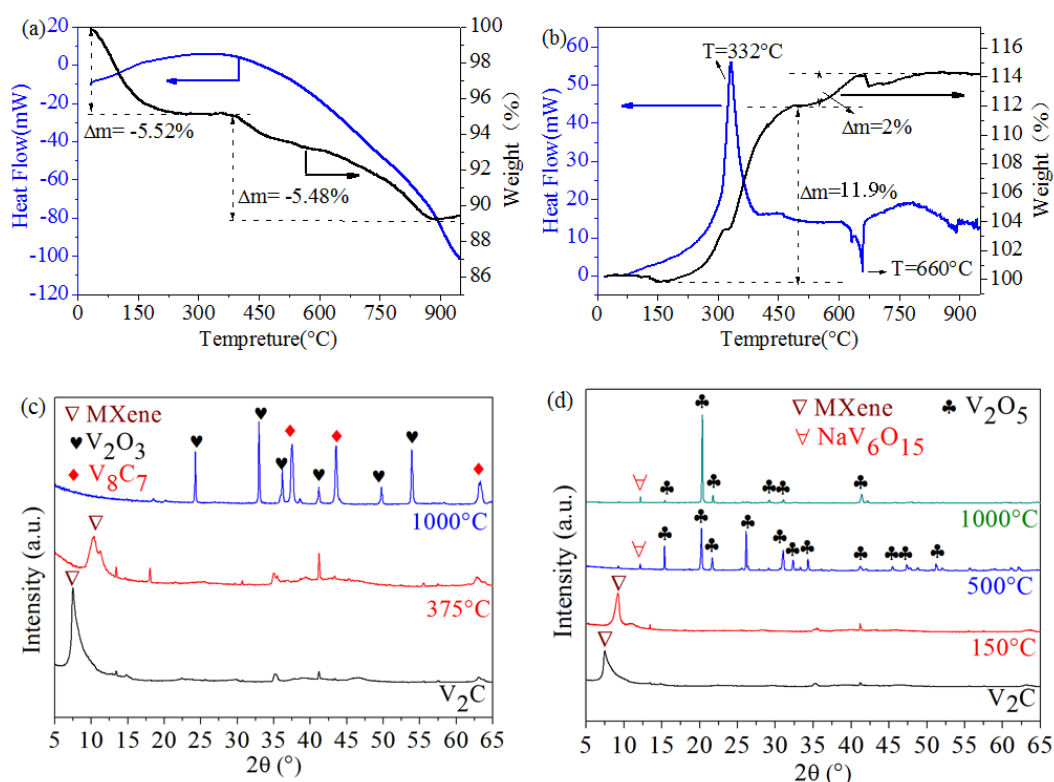


Figure 3. TG and DTA curves of V_2C MXene in (a) Ar atmosphere and (b) air atmosphere. XRD patterns of V_2C MXene samples after heat treatment in (c) Ar atmosphere and (d) air atmosphere.

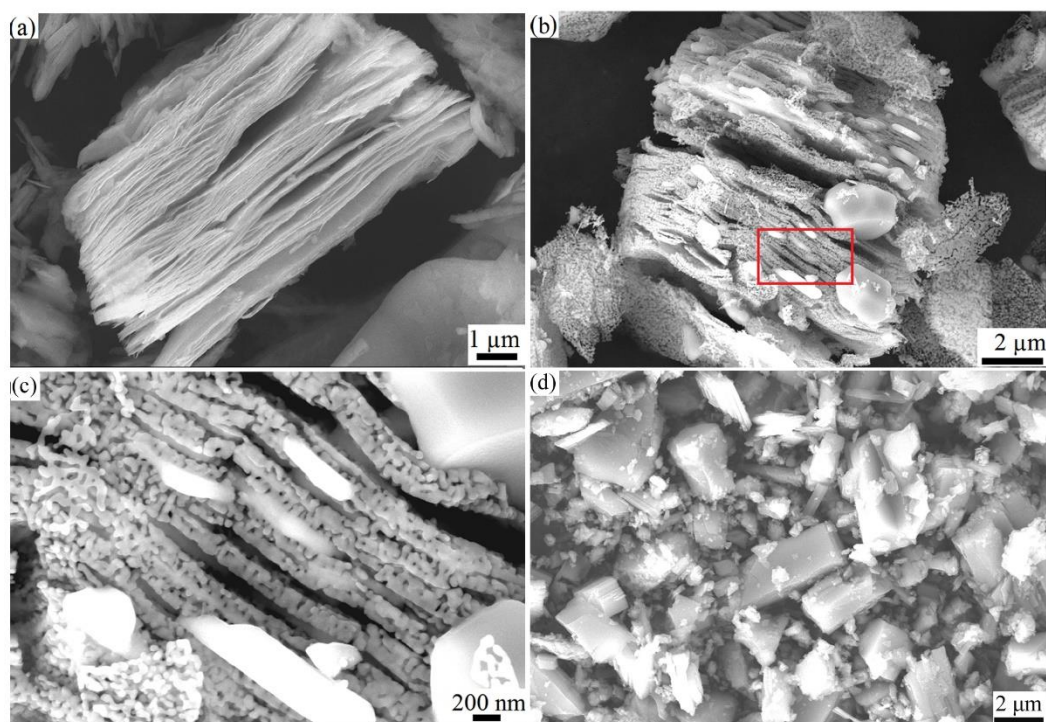


Figure 4. SEM images of V_2C MXene after heat treatment at (a) 150 °C in Ar; (b) 1000 °C in Ar; (c) is a highly magnification image of area in the red rectangle of b; (d) at 1000 °C in air.

(1) Thermal Stability in Ar

In Ar atmosphere, the TG curve of V_2C MXene in Figure 3a is divided into two stages. The first stage is 5.52% weight loss from RT to 375 °C. Most of the weight loss occurred in the temperature range of 70–120 °C, which is due to the loss of physically adsorbed water. The DTA curve at this temperature range does not display obvious change. Additionally, the structure of MXene has not changed. The second stage is 5.48% weight loss from 375 °C to 900 °C, which is caused by the loss of OH/O/F terminated groups. The weight loss needs energy to break the bonds between OH/O/F and V_2C crystals. Thus, the corresponding DTA curve is obviously endothermic. In this process, OH/O/F are released in the form of $H_2O/O_2/HF$. At high temperatures (>900 °C), almost all terminated groups have already been lost; therefore, the weight loss stops. At such a high temperature, V_2C reacts with previously released oxygen to form oxides. Thus, there is a weak weight gain. According to this analysis, the heat process of V_2C in Ar is mainly a weight loss process at a low temperature and a weak weight gain at a temperature >900 °C.

The conclusion drawn from Figure 3a can be supported by the XRD patterns in Figure 3c and the SEM micrographs in Figure 4. In Figure 3c, after heating at 375 °C in Ar, the sample's main composition was still V_2C MXene. The physically adsorbed water and some surface terminations were lost, and the interlayer distance of V_2C MXene was reduced. As shown in Figure 3c, the 2θ angle of the (002) peak shifted from 9.172° to 10.35°, which means that the d space of the basal plane, including the thickness of the V_2C layer and interlayer distance, was reduced from 0.963 nm to 0.854 nm. This reduction of the value was due to the reduction of the interlayer distance. After heat treatment at 1000 °C, some V_2C was oxidized to form V_2O_3 , and some V_2C was transformed to V_8C_7 .

From the SEM image in Figure 4a, 150 °C treatment did not change the 2D structure of V_2C MXene. From Figure 4b,c, however, 1000 °C treatment obviously changed the 2D structure of V_2C MXene. A large number of nanoparticles appeared and were distributed on the surface and in the interlayer space of the multilayered 2D structure. From EDS, the particles consisted of V and O elements, and the element ratio was 2.1:2.9, so it can be confirmed that these particles were V_2O_3 . This result agrees with the XRD patterns in Figure 3c.

The derived material consisted of V_2O_3 nanoparticles distributed in the 2D structure. The vanadium oxide had a very high specific surface area. Vanadium oxide is used as a catalyst in many areas. If the composition and structure can be better controlled, the derived material can be applied as a catalyst with a high performance.

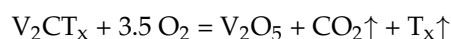
(2) Thermal Stability in Air

In air atmosphere, as shown in Figure 3b, the first stage of the TG curve shows a weak weight loss (RT to 150 °C) due to the loss of physically adsorbed water. As shown in Figure 3d, the XRD pattern of V_2C does not display obvious change, except for the fact that the (002) peak shifts to a high angles direction.

With the temperature rising, the surface of V_2C begins to be oxidized in air atmosphere. Therefore, there is a large exothermic peak at 332 °C in the DTA curve and a drastic weight gain in the TG curve (Figure 3b). According to the XRD pattern in Figure 3d, the oxidation product is V_2O_5 rather than V_2O_3 , because there is enough oxygen in air atmosphere. After the exothermic peak at 332 °C, there is an endothermic peak at ~660 °C, which corresponds the melt of newly formed V_2O_5 (the melting point of pure V_2O_5 is 690 °C [31]). Therefore, there is an exothermic peak (332 °C) and an endothermic peak (660 °C) in the DTA curve of V_2C .

According to the XRD and SEM results in Figures 3d and 4d, the oxidation products of V_2CT_x in air at 1000 °C are a lot of V_2O_5 crystals in a rectangular block shape and a small amount of NaV_6O_{15} [32].

The following reaction is proposed to describe the oxidation of V_2CT_x in air:



4. Conclusions

Based on the research in this paper, it is concluded that only NaF + HCl etching solution can be used to synthesize highly pure V_2C MXene. Neither LiF + HCl nor KF + HCl can be used. The existence of Na^+ and Cl^- in etching solution is essential for the synthesis of highly pure V_2C . The chemical reason for this is related to the radius of hydrated cations and the solubility fluoride salts. From the radius of hydrated cations, $Na^+ > K^+$; from the solubility, $NaF > LiF$. Thus, Na^+ has a better exfoliation ability than Li^+ and K^+ . Additionally, NaF has a better solubility in NaF + HCl solution than in NaF + HF solution. Thus, NaF + HCl has a better exfoliation ability than NaF + HF. The suitable condition is etching in NaF + HCl solution at 90 °C for 72 h.

The synthesized V_2C MXene was stable in Ar atmosphere below 375 °C; above this temperature, V_2C was oxidized to form V_2O_3 nano-crystals, which were evenly distributed on 2D V_2C sheets. In air, V_2C maintained a stable 2D structure at 150 °C; above this temperature, V_2C was oxidized and V_2O_5 was the final oxidized product.

Author Contributions: Conceptualization & Supervision: Q.H., L.W., and A.Z.; Methodology: M.W., B.W., and A.Z.; Analysis: B.W. and A.Z.; Writing and Editing: M.W., B.W., and A.Z.

Funding: This work was supported by National Natural Science Foundation of China (Grant numbers 51772077, 51472075), Natural Science Foundation of Henan Province (Grant numbers 182300410228, 182300410275), and Program for Innovative Research Team (in Science and Technology) at the University of Henan Province (19IRTSTHN027).

Conflicts of Interest: The authors declare no conflict of interest.

References

1. Naguib, M.; Kurtoglu, M.; Presser, V.; Lu, J.; Niu, J.; Min, H.; Hultman, L.; Gogotsi, Y.; Barsoum, M.W. Two-dimensional nanocrystals produced by exfoliation of Ti_3AlC_2 . *Adv. Mater.* **2011**, *23*, 4207. [CrossRef]
2. Ying, G.; Dillon, A.D.; Fafarman, A.T.; Barsoum, M.W. Transparent, conductive solution processed spincoated 2D Ti_3AlC_2 . (MXene) films. *Mater. Res. Lett.* **2017**, *5*, 391–398. [CrossRef]

3. Zhi, W.S.; Fredrickson, K.D.; Anasori, B.; Kibsgaard, J.; Strickler, A.L.; Lukatskaya, M.R.; Gogotsi, Y.; Jaramillo, T.F.; Vojvodic, A. Two-dimensional molybdenum carbide (MXene) as an efficient electrocatalyst for hydrogen evolution. *ACS Energy Lett.* **2016**, *1*, 589–594. [[CrossRef](#)]
4. Naguib, M.; Halim, J.; Lu, J.; Cook, K.M.; Hultman, L.; Gogotsi, Y.; Barsoum, M.W. New two-dimensional niobium and vanadium carbides as promising materials for li-ion batteries. *J. Am. Chem. Soc.* **2013**, *135*, 15966–15969. [[CrossRef](#)] [[PubMed](#)]
5. Zhang, X.; Xue, M.; Yang, X.; Wang, Z.; Luo, G.; Huang, Z.; Sui, X.; Li, C. Preparation and tribological properties of $Ti_3C_2(OH)_2$ nanosheets as additives in base oil. *Rsc. Adv.* **2014**, *5*, 2762–2767. [[CrossRef](#)]
6. Ling, C.; Li, S.; Ouyang, Y.; Chen, Q.; Wang, J. Transition metal-promoted V_2CO_2 (MXenes): A new and highly active catalyst for hydrogen evolution reaction. *Adv. Sci.* **2016**, *3*, 1600180. [[CrossRef](#)] [[PubMed](#)]
7. Liu, Y.; Zhang, X.; Dong, S.; Ye, Z.; Wei, Y. Synthesis and tribological property of $Ti_3C_2T_x$ nanosheets. *J. Mater. Sci.* **2017**, *52*, 2200–2209. [[CrossRef](#)]
8. Wu, Y.; Nie, P.; Jiang, J.; Ding, B.; Dou, H.; Zhang, X. MoS_2 -Nanosheet- Decorated 2D titanium carbide (MXene) as high-performance anodes for sodium-ion batteries. *Chem. Electro. Chem.* **2017**, *4*, 1560–1565. [[CrossRef](#)]
9. Li, X.; Qian, Y.; Liu, T.; Cao, F.; Zang, Z.; Sun, X.; Sun, S.; Niu, Q.; Wu, J. Enhanced lithium and electron diffusion of $LiFePO_4$ cathode with two-dimensional Ti_3C_2 MXene nanosheets. *J. Mater. Sci.* **2018**, *53*, 1–13. [[CrossRef](#)]
10. Wang, F.; Wang, Z.; Zhu, J.; Yang, H.; Chen, X.; Wang, L.; Yang, C. Facile synthesis SnO_2 nanoparticle-modified Ti_3C_2 MXene nanocomposites for enhanced lithium storage application. *J. Mater. Sci.* **2016**, *52*, 1–10. [[CrossRef](#)]
11. Sun, D.; Wang, M.; Li, Z.; Fan, G.; Fan, L.Z.; Zhou, A. Two-dimensional Ti_3C_2 as anode material for Li-ion batteries. *Electrochem. Commun.* **2014**, *47*, 80–83. [[CrossRef](#)]
12. Ran, J.; Gao, G.; Li, F.T.; Ma, T.Y.; Du, A.; Qiao, S.Z. Ti_3C_2 MXene co-catalyst on metal sulfide photo-absorbers for enhanced visible-light photocatalytic hydrogen production. *Nat. Commun.* **2017**, *8*, 13907. [[CrossRef](#)] [[PubMed](#)]
13. Guo, Z.; Zhou, J.; Zhu, L.; Sun, Z. MXene: A promising photocatalyst for water splitting. *J. Mater. Chem. A* **2016**, *4*, 11446–11452. [[CrossRef](#)]
14. Sun, D.; Hu, Q.; Chen, J.; Zhang, X.; Wang, L.; Wu, Q.; Zhou, A. Structural Transformation of MXene (V_2C , Cr_2C , and Ta_2C) with O Groups during Lithiation: A First-Principles Investigation. *ACS Appl. Mater. Interfaces* **2016**, *8*, 74–81. [[CrossRef](#)] [[PubMed](#)]
15. Dall’Agnese, Y.; Taberna, P.L.; Gogotsi, Y.; Simon, P. Two-dimensional vanadium carbide (MXene) as positive electrode for sodium-ion capacitors. *J. Phys. Chem. Lett.* **2015**, *6*, 2305–2309. [[CrossRef](#)] [[PubMed](#)]
16. Wang, B.; Zhou, A.; Liu, F.; Cao, J.; Wang, L.; Hu, Q. Carbon dioxide adsorption of two-dimensional carbide MXenes. *J. Adv. Ceram.* **2018**, *7*, 237–245. [[CrossRef](#)]
17. Sun, D.D.; Hu, Q.K.; Chen, J.F.; Zhou, A.G. First principles calculations of the relative stability, structure and electronic properties of two dimensional metal carbides and nitrides. *Key Eng. Mater.* **2014**, *602–603*, 527–531. [[CrossRef](#)]
18. Yang, J.; Chen, B.; Song, H.; Tang, H.; Li, C. Synthesis, characterization, and tribological properties of two-dimensional Ti_3C_2 . *Cryst. Res. Technol.* **2014**, *49*, 926–932. [[CrossRef](#)]
19. Chen, J.; Chen, K.; Tong, D.; Huang, Y.; Zhang, J.; Xue, J.; Huang, Q.; Chen, T. CO_2 and temperature dual responsive “Smart” MXene phases. *Chem. Commun.* **2015**, *51*, 314–317. [[CrossRef](#)] [[PubMed](#)]
20. Zhou, J.; Gao, S.; Guo, Z.; Sun, Z. Ti-enhanced exfoliation of V_2AlC into V_2C MXene for lithium-ion battery anodes. *Ceram. Int.* **2017**, *43*, 11450–11454. [[CrossRef](#)]
21. Liu, F.; Zhou, J.; Wang, S.; Wang, B.; Shen, C.; Wang, L.; Hu, Q.; Huang, Q.; Zhou, A. Preparation of high-purity V_2C MXene and electrochemical properties as li-ion batteries. *J. Electrochem. Soc.* **2017**, *164*, A709–A713. [[CrossRef](#)]
22. Anasori, B.; Lukatskaya, M.R.; Gogotsi, Y. 2D metal carbides and nitrides (MXenes) for energy storage. *Nat. Rev. Mater.* **2017**, *2*, 16098. [[CrossRef](#)]
23. Li, Z.; Wang, L.; Sun, D.; Zhang, Y.; Liu, B.; Hu, Q.; Zhou, A. Synthesis and thermal stability of two-dimensional carbide MXene Ti_3C_2 . *Mater. Sci. Eng. B.* **2015**, *191*, 33–40. [[CrossRef](#)]

24. Zhou, J.; Zha, X.; Chen, F.Y.; Ye, Q.; Eklund, P.; Du, S.; Huang, Q. A Two-Dimensional Zirconium Carbide by Selective Etching of Al_3C_3 from Nanolaminated $\text{Zr}_3\text{Al}_3\text{C}_5$. *Angew. Chem.* **2016**, *55*, 5008–5013. [[CrossRef](#)] [[PubMed](#)]
25. Wang, B.; Zhou, A.; Hu, Q.; Wang, L. Synthesis and oxidation resistance of V_2AlC powders by molten salt method. *Int. J. Appl. Ceram. Tec.* **2017**, *14*, 873–879. [[CrossRef](#)]
26. Duan, X.; Wu, C.; Xiang, S.; Zhou, W.; Yildirim, T.; Cui, Y.; Yang, Y.; Chen, B.; Qian, G. Novel microporous metal-organic framework exhibiting high acetylene and methane storage capacities. *Inorg. Chem.* **2015**, *54*, 4377–4381. [[CrossRef](#)] [[PubMed](#)]
27. Naguib, M.; Mashtalir, O.; Carle, J.; Presser, V.; Lu, J.; Hultman, L.; Gogotsi, Y.; Barsoum, M.W. Two-dimensional transition metal carbides. *ACS Nano.* **2012**, *6*, 1322–1331. [[CrossRef](#)] [[PubMed](#)]
28. Ghidui, M.; Lukatskaya, M.R.; Zhao, M.Q.; Gogotsi, Y.; Barsoum, M.W. Conductive two-dimensional titanium carbide ‘clay’ with high volumetric capacitance. *Nature* **2014**, *516*, 78–81. [[CrossRef](#)] [[PubMed](#)]
29. Spanier, J.E.; Gupta, S.; Amer, M.; Barsoum, M.W. Vibrational behavior of the $\text{M}_{n+1}\text{AX}_n$ phases from first-order raman scattering ($\text{M} = \text{Ti}, \text{V}, \text{Cr}$, $\text{A} = \text{Si}$, $\text{X} = \text{C}, \text{N}$). *Phys. Rev. B* **2005**, *71*, 012103. [[CrossRef](#)]
30. Champagne, A.; Lu, S.; Ouisse, T.; Hackens, B.; Charlier, J.C. Electronic and vibrational properties of V_2C -based MXenes: From experiments to first-principles modeling. *Phys. Rev. B* **2017**, *97*, 115439. [[CrossRef](#)]
31. Wu, Y.P.; Ong, C.K.; Li, Z.W.; Chen, L.; Lin, G.Q.; Wang, S.J. Microstructural and high-frequency magnetic characteristics of W -type barium ferrites doped with V_2O_5 . *J. Appl. Phys.* **2005**, *97*, 1294. [[CrossRef](#)]
32. Zhang, H.; Wang, L.; Shen, C.; Qin, G.; Hu, Q.; Zhou, A. Synthesis of $\text{NaV}_6\text{O}_{15}$ nanorods via thermal oxidation of sodium-intercalated $2d \text{V}_2\text{CT}_x$ and their electrochemical properties as anode for lithium-ion batteries. *Electrochim. Acta* **2017**, *248*, 178–187. [[CrossRef](#)]



© 2018 by the authors. Licensee MDPI, Basel, Switzerland. This article is an open access article distributed under the terms and conditions of the Creative Commons Attribution (CC BY) license (<http://creativecommons.org/licenses/by/4.0/>).